Oleate-Induced Beta Cell Dysfunction and Apoptosis: A Proteomic Approach to Glucolipotoxicity by an Unsaturated Fatty Acid

ARTICLE *in* JOURNAL OF PROTEOME RESEARCH · JUNE 2011

Impact Factor: 4.25 · DOI: 10.1021/pr101290n · Source: PubMed

9 AUTHORS, INCLUDING:

Wannes D'Hertog
Karel de Grote-Hogeschool
22 PUBLICATIONS **452** CITATIONS
SEE PROFILE

Hannelie Korf
University of Leuven
35 PUBLICATIONS **1,166** CITATIONS
SEE PROFILE

Tatsuro Koike
Hokkaido University
105 PUBLICATIONS **2,151** CITATIONS
SEE PROFILE

Chantal Mathieu
University of Leuven
246 PUBLICATIONS **10,811** CITATIONS
SEE PROFILE

Journal of proteome research

ARTICLE

pubs.acs.org/jpr

Oleate-Induced Beta Cell Dysfunction and Apoptosis: A Proteomic Approach to Glucolipotoxicity by an Unsaturated Fatty Acid

Michael Maris,[†] Etienne Waelkens,[‡,§] Miriam Cnop,[∥,⊥] Wannes D'Hertog,[†] Daniel A. Cunha,[∥] Hannelie Korf,[†] Tatsuro Koike,[#] Lut Overbergh,[*,†] and Chantal Mathieu[†]

[†]Laboratory for Experimental Medicine and Endocrinology (LEGENDO), Herestraat 49, Catholic University of Leuven, Leuven, Belgium

[‡]Laboratory of Protein Phosphorylation and Proteomics, Catholic University of Leuven, Leuven, Belgium

[§]ProMeta, Catholic University of Leuven, Leuven, Belgium

[∥]Laboratory of Experimental Medicine, Université Libre de Bruxelles (ULB), Route de Lennik, 808, 1070 Brussels, Belgium

[⊥]Division of Endocrinology, Erasmus Hospital, Université Libre de Bruxelles (ULB), Route de Lennik, 1070 Brussels, Belgium

[#]Molecular Neurobiology Lab, Graduate School of Life Science, Hokkaido University, Japan

Supporting Information

ABSTRACT: High levels of fatty acids contribute to loss of functional beta cell mass in type 2 diabetes, in particular in combination with high glucose levels. The aim of this study was to elucidate the role of the unsaturated free fatty acid oleate in glucolipotoxicity and to unravel the molecular pathways involved. INS-1E cells were exposed to 0.5 mM oleate, combined or not with 25 mM glucose, for 24 h. Protein profiling of INS-1E cells was done by 2D-DIGE, covering pH ranges 4−7 and 6−9 ($n = 4$). Identification of differentially expressed proteins ($P < 0.05$) was based on MALDI-TOF analysis using Peptide Mass Fingerprint (PMF) and fragmentation (MS/MS) of the most intense peaks of PMF and proteomic results were confirmed by functional assays. Oleate impaired glucose-stimulated insulin secretion and decreased insulin content. 2D-DIGE analysis revealed 53 and 54 differentially expressed proteins for oleate and the combination of oleate and high glucose, respectively. Exposure to oleate down-regulated chaperones, hampered insulin processing and ubiquitin-related proteasomal degradation, and induced perturbations in vesicle transport and budding. In combination with high glucose, shunting of excess amounts of glucose toward reactive oxygen species production worsened beta cell death. The present findings provide new insights in oleate-induced beta cell dysfunction and identify target proteins for preservation of functional beta cell mass in type 2 diabetes.

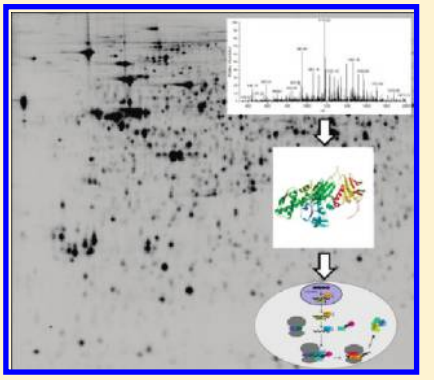

KEYWORDS: lipotoxicity, beta cells, oleate, type 2 diabetes, proteomics

INTRODUCTION

Type 2 diabetes (T2D) is a dual disease characterized by peripheral insulin resistance and insufficient compensation of insulin secretion by the pancreatic beta cells. Both beta cell dysfunction and actual decrease in beta cell mass have been implicated in this deterioration of functional beta cell capacity.[1] Genetic as well as environmental factors contribute to the pathogenesis of type 2 diabetes, but the disturbed fuel mixture circulating in type 2 diabetic patients, characterized by high glucose and high free fatty acid levels, contributes to further progression of the disease. Free fatty acids (FFA) play a primordial role in the induction of insulin resistance in skeletal muscle and liver[2,3] as well as in the dysfunction of adipocytes, further worsening insulin resistance.[4] FFA also cause beta cell dysfunction and death, that is, lipotoxicity,[5] a phenomenon that is amplified in combination with high glucose, that is, glucolipotoxicity.[6]

Most studies have focused on saturated FFA, to which many cytotoxic effects are attributed. The role of unsaturated FFA is less studied and more controversial. Studies in the RIN beta cell line have shown a cytoprotective effect of unsaturated FFA through the blockade of apoptosis and the promotion of beta cell proliferation, independently of oleate metabolism.[7−9] Oleate, the most common unsaturated FFA in human plasma, had no cytoprotective effects in the INS-1E beta cell line, but it induced less apoptosis than saturated FFA. Oleate induces a milder activation of the unfolded protein response (UPR), but it induces the release of cytochrome c and apoptosis-inducing factor (AIF), and the accumulation of cytosolic caspase-2.[10−12] The oleate-induced dysfunction seen in the INS-1E cell line was confirmed in pancreatic islets, which have impaired glucose-stimulated insulin secretion (GSIS) after exposure to oleate.[13−15] These oleate-treated islets also showed elevated glucagon release that may aggravate the hyperglycaemic effects *in vivo*.[16]

Received: December 28, 2010
Published: June 27, 2011

Busch et al. performed a microarray study of oleate-exposed MIN6 cells and found 62 genes as being altered ≥1.9 fold. Genes involved in inflammation and acute phase response, as well as transcriptional modulators, were increased by oleate.[17] As there is often a poor correlation between the abundance of mRNA and the levels of their encoded proteins, which mediate cellular functions, and because microarrays do not detect post-transcriptional events, studying the proteome profile is indispensable. Ortsäter et al. profiled the proteome of pancreatic islets, exposed to glucose and oleate for 24 and 48 h. The expression level of 25 proteins was altered between the several conditions, but due to the use of the SELDI-TOF technique, they were only able to identify one protein, namely peptidyl-prolyl isomerase B.[18] As a result, to date, information about the exact molecular pathways, induced by oleate in beta cells, is lacking.

The aim of the present study was to perform global protein profiling using the sensitive 2D-DIGE approach in order to reveal the many pathways in beta cells that are affected by oleate, combined or not with high glucose. As pancreatic islets consist of several cell types, we chose to use the rat insulin producing INS-1E cell line, an accepted model of pancreatic beta cells.[19]

We demonstrate that the unsaturated FFA oleate exerts detrimental effects on beta cells by down-regulation of protective chaperone proteins, hampered insulin processing, as well as impeded ubiquitin-associated degradation and vesicle transport and budding. In combination with high glucose, fatty acid synthesis was promoted with the generation of harmful side-products and excess glucose was shunted toward pathways that generate reactive oxygen species (ROS). These protein changes may disrupt proper cellular function, leading to the accumulation of unprocessed insulin and reducing mature insulin stores and insulin secretion.

METHODS

INS-1E Cell Culture Conditions

The rat insulin-producing INS-1E cell line, a kind gift from Prof. C. Wollheim (Centre Medical Universitaire, Geneva, Switzerland), was cultured in RPMI1640 (with GlutaMAX-I) (Invitrogen, Merelbeke, Belgium) containing 10% heat-inactivated fetal calf serum (FCS), 10 mM HEPES, 1 mM sodium pyruvate, 100 U/mL penicillin, 100 μg/mL streptomycin and 50 μM 2-mercapto ethanol.[20] INS-1E cells were cultured in the above-mentioned medium for 72 h and were then exposed to 11 mM glucose (control) or 0.5 mM oleate, combined or not with 25 mM glucose. Oleate (Sigma, Bornem, Belgium) was dissolved in 90% ethanol, heated to 60 °C and used in a 1:100 dilution (at a final concentration of 0.5 mM) in RPMI 1640 medium with 1% bovine serum albumin (BSA) and 1% FCS. Cells used for experiments ranged from passage 62 to 76.

Cell Death Analysis

The percentage of living, apoptotic and necrotic INS-1E cells was assessed by microscopic counting as described.[21] Cells were incubated for 15 min with propidium iodide (PI; 10 μg/mL) and Hoechst 33342 (HO342; 20 μg/mL). A minimum of 500 cells was counted in each experimental condition on an inverted fluorescent Ti-E microscope (Nikon, Brussels, Belgium). Viable or necrotic cells were identified by intact nuclei with, respectively, blue (HO342) or yellow (HO342 plus PI) fluorescence. Apoptotic cells were detected by their fragmented nuclei which exhibited either a blue or yellow fluorescence depending on the stage in the process. In addition, apoptosis was also assessed by the measurement of DNA fragmentation with the Cell Death Detection ELISA plus kit (Roche Diagnostics, Vilvoorde, Belgium) and by the measurement of caspase 3 and 7 activation with the Caspase-Glo 3/7 assay (Promega, Madison, WI).

Two-Dimensional Difference Gel Electrophoresis (2D-DIGE)

2D-DIGE was performed as previously described.[22] In short, 5×10^6 INS-1E cells were exposed to 11 mM glucose (control) or 0.5 mM oleate, combined or not with 25 mM glucose, for 24 h. For each condition, quadruplicate experiments were performed, originating from four independent experiments. The cells were washed twice in PBS and resuspended in 100 μL lysis buffer (7 M urea, 2 M thiourea, 4% CHAPS, 40 mM Tris base, 1% DTT and a mixture of protease inhibitors (Complete protease inhibitor, Roche Diagnostics, Vilvoorde, Belgium)). Samples were sonicated and the supernatant was desalted by dialysis (PlusOne Mini Dialysis kit, GE Healthcare, Diegem, Belgium). Fifty micrograms of protein were labeled with Cy3 or Cy5, and a pooled internal standard was labeled with Cy2. Dye swapping made sure that each condition was equally labeled with Cy3 or Cy5, eliminating potential bias from the labeling reaction. A schematic table, presenting the gels samples, labels and pooled standards is provided in the Supporting Information. For the first dimension, pooled samples, containing sample loading buffer, were loaded onto the rehydrated IPG strips (24 cm) (GE Healthcare) using anodic cup loading and separated according to their isoelectric point on an Ettan IPGphorII manifold (GE Healthcare). The first dimension was ended when the current reached a stable phase (at ∼60 kV.h). The following parameters during isoelectric focusing were applied:

pH 4−7				pH 6−9			
steps	step/gradient	voltage	hours (h)	steps	step/gradient	voltage	hours (h)
1	Step	150	1.5	1	Gradient	150	1.5
2	Gradient	300	1	2	Step	500	1
3	Gradient	1000	3	3	Gradient	1000	5
4	Gradient	8000	1	4	Gradient	8000	3
5	Step	8000	10	5	Step	8000	9
6	Step	200	7	6	Step	400	7

Prior to the second dimension, the strips were equilibrated during two intervals of 15 min each in an equilibration buffer (7 M urea, 2 M thiourea, 4% CHAPS, 0.5% IPG buffer, 0.05% OrangeG), and either 1% DTT (for IPG strips pH 4−7) or 1.2% Destreak (for IPG strips pH 6−9) and the equilibrated strips were placed on top of 12.5% SDS-polyacrylamide gel (24 × 20 cm) and separated on an Ettan DaltSix system (GE Healthcare) at 8 mA/gel, 9 W and 600 V for 1 h and then at 16 mA/gel, 15 W and 600 V until the bromophenol blue dye front reached the bottom of the gel.

Scanning of the gels was performed using a Typhoon9400 (GE Healthcare). Initial scan parameters were press sample, depth plus 3 mm, 500 to 550 V photomultiplier tube setting and 1000-μm pixel size, before repeating at 100-μm pixel size for a high-resolution scan. Spot detection and matching was performed automatically using the BVA module of DeCyder Version 7.0 software followed by careful manual rematching of wrongly matched spots or unmatched spots. Spot detection

parameters were set as described by the manufacturer: spot detection algorithm 6.0, estimated number of spots: 10 000 and spot volumes below 30 000 were excluded. The 12 spot maps corresponding to the 4 gels from each pH range were used to calculate average abundance. Protein spot expression levels which showed a statistically significant ($P < 0.05$) increase or decrease in 6 out of 8 (Cy3 or Cy5 labeled) gels were accepted as being differentially expressed.

Spot Digestion and Protein Identification by MALDI-TOF/TOF Analysis

For spot picking, two preparative gels for each pH range were run (350 μg protein lysate each). Similar electrophoretic parameters for first and second dimension runs were used as for analytical gels, except that Cy dye-labeling was omitted. Glass plates (27 × 21 cm) were pretreated with BindSilane and two reference markers were applied to enable automatic picking. The gels (24 × 20 cm) were poststained using Krypton (Pierce, Rockford, IL, USA). Matching with the analytical gels was performed using the BVA module of the DeCyder V7.0 software. A pick list was generated and exported into the Spot Picker V1.20 software, which controls the Ettan Spot Picker (GE Healthcare). Spot digestion and peptide purification was performed as previously reported.[23] MS/MS analyses were performed on a 4800 MALDI TOF/TOF (Applied Biosystems, Foster City, CA). The instrument was calibrated with the Applied Biosystems Calibration Mixture 1. The mass accuracy (external calibration) was <50 ppm in reflectron mode. Measurements were taken in the positive ion mode between 900 and 3000 m/z. Sequences were automatically acquired by scanning first in MS mode and selecting the 15 most intense ions for MS/MS using an exclusion list of peaks arising from tryptic autodigestion. Air was used as the collision gas, while the collision energy was adapted automatically. Data interpretation was carried out using GPS Explorer software (V3.6), and database searching was carried out using Mascot (version 2.2.00). The following raw data extraction parameters used by GPS explorer in order to extract mascot compatible files were used: mass range: 900−3500 Da; peak intensity: maximum 10 peaks per 200 Da; minimum signal-to-noise: 5; minimum area: 100 and max peak/spot: 50. Since all experiments were performed on rat INS-1E cells, MS/MS searches were conducted with the following settings: UniProt_sprot (517 100 sequences; 182 146 551 residues, release date June 2010) with the taxonomy set on Rattus (7512 sequences). For protein identifications where no hit was found in the rat databases, protein identity was based on comparison with the orthologous mouse sequence because the mouse genome is better annotated compared with the rat genome. MS/MS tolerance for precursor ions was set on 1 Da and for fragment ions on 1 Da; methionine oxidation was used as a variable modification and carbamidomethylation of cysteine as a fixed modification. An estimation of the FDR, based on a decoy base, was done on all identifications. As enzyme, trypsin was selected and a maximum of one missed cleavage was allowed. Using these parameters, only peptides that match above identity threshold were retained and the probability-based MOWSE scores greater than the given cutoff value for MS/MS fragmentation data were taken as significant ($P < 0.05$). All additional mass spectrometric information of the individual peptide sequences, as well as the FDR are shown in the supplementary Tables 1 and 2.

For all identified proteins, each sequenced peptide was individually aligned using BLAST.[24] In case more than one protein is present in a single spot, the different names/accession numbers are reported and indicated with an asterix (*). Although the majority of protein identifications are based on multiple peptide sequences, some identifications are single peptide-based protein identifications. In this case, alignment using BLAST rules out that this single peptide is a unique peptide of a certain protein. Additionally, the associated MS/MS spectra are shown in the Supporting Information.

Glucose-Stimulated Insulin Secretion

INS-1E cells were seeded in 24 well plates (100 000 cells/well) and treated with 0.5 mM oleate at 11 or 25 mM glucose for 24 h. Cells were incubated with glucose-free medium for 2 h. Next, cells were washed twice with prewarmed glucose-free Krebs-Ringer bicarbonate (KRB) buffer (10 mM Hepes (pH 7.4); 90 mM NaCl; 5 mM $NaHCO_3$; 4.8 mM KCl; 0.7 mM KH_2PO_4; 0.6 mM $MgSO_4$; 2.5 mM $CaCl_2$ and 0.1% BSA) and equilibrated for 30 min at room temperature in glucose-free KRB. Thereafter, the buffer was removed and cells were exposed to KRB solution containing 3 mM or 30 mM glucose for 1 h at 37 °C. At the end of this incubation period, supernatant and cells were collected for (pro)insulin assay.

Pro-insulin and insulin were determined on buffer and acid ethanol-extracted cells using, respectively, rat pro-insulin and rat insulin enzyme-linked immunosorbent assay (ELISA) kits (Mercodia, Uppsala, Sweden). Cellular (pro)insulin content was normalized to total DNA content.[25]

Western Blot Analysis

INS-1E cells were lysed in whole cell extract buffer (150 mM NaCl, 50 mM NaF, 1 mM $MgCl_2$, 1 mM $CaCl_2$, 1% Nonidet P-40, 1 mM Na_3VO_4, 1 mM phenylmethylsulfonyl fluoride, and complete protease inhibitor mixture) for 15 min on ice. Total cell lysate was sonicated, centrifuged (15 min at 14 000 rpm) and the supernatant was used for Western blot analysis. The protein samples were separated on a 4−12% BT gel (Invitrogen), blotted onto a nitrocellulose membrane (Hybond-ECL; GE Healthcare) and probed with a rabbit antibody against PC2 (1:100 dilution; Millipore, Brussels, Belgium) or GRP78 (1:2000 dilution; Cell Signaling, Beverly, MA) and a mouse antibody against beta actin (1:12 000 dilution; Sigma) or alfa tubulin (1:10 000 dilution; Sigma) as primary antibodies. Secondary goat antimouse and antirabbit antibodies, labeled with the fluorescent dyes Cy3 or Cy5 (GE Healthcare) were added in a 1:5000 dilution. Membranes were air-dried, scanned using a Typhoon 9400 (GE Healthcare) and quantified using ImageQuant analysis software (GE Healthcare).

Adenoviral Restoration of GRP78 Expression

The adenovirus encoding rat GRP78 (Ad-GRP78) was generated by insertion of the full-length rat GRP78 cDNA in a cosmid vector Ax1CAwt. Control adenovirus encoding luciferase (Ad-LUC) was from Vector Biolabs (Philadelphia, PA, USA). INS-1E cells were incubated in medium containing Ad-LUC or Ad-GRP78 at a multiplicity of infection of 1 for 2 h at 37 °C. After 24 h, cells were treated as indicated. Transfection with the adenovirus encoding rat GRP78 induced a 3.4 ± 0.4 fold increase in GRP78 expression as compared to transfection with the control adenovirus ($P < 0.01$).

Table 1. List of Oleate-Modified Proteins[a]

spot no	Swiss-Prot ID	protein	ion score	peptides matched above identity threshold	percentage sequence coverage	pH range	fold regulation
		Metabolism					
279	P16638	ATP-citrate synthase	264	6	8.00%	6−9	−1.48
822*	P35571	Glycerol-3-phosphate dehydrogenase, mitochondrial	178	3	7.29%	4−7	1.34
1156	P10860	glutamate dehydrogenase	96	2	5.73%	6−9	1.36
1205	P15999	ATP synthase subunit alpha, mitochondrial	406	6	17.54%	6−9	1.65
1408	Q9DBF1	Alpha-aminoadipic semialdehyde dehydrogenase	151	3	11.87%	4−7	1.34
1432	Q6DGF1	Isocitrate dehydrogenase, mitochondrial	357	8	21.68%	6−9	1.37
1649	P04764	Alpha - enolase	259	4	16.59%	4−7	−1.26
		Beta - enolase	169	2	8.53%	4−7	−1.26
2252	Q499R7	Ppa1 protein	311	5	21.75%	4−7	−1.21
2539	Q9Z339	Glutathione transferase omega-1	382	7	35.68%	4−7	1.58
2721	P16617	phosphoglycerate kinase	110	2	8.87%	4−7	1.24
2735	Q9DCT2	NADH dehydrogenase (ubiquinone) Fe−S protein 3	77	2	10.65%	4−7	1.13
2782	O35760	isopentenyl-diphosphate delta isomerase	117	3	20.70%	4−7	−1.45
		Protein folding					
822*	Q5XHZ0	Heat shock protein 75 kDa, mitochondrial	126	3	7.22%	4−7	1.34
930	P63018	Heat shock 70 kDa ptotein 8	549	9	24.30%	4−7	−1.18
1209*	P63039	60 kDa heat shock protein, mitochondrial precursor	642	7	22.34%	4−7	−1.25
1744	P06761	78 kDa glucose-regulated protein precursor (GRP 78)	127	3	9.02%	4−7	−1.51
1901	Q66H09	tetratricopeptide repeat domain 1	43	1	4.11%	4−7	−1.23
1998*	P11598	Protein disulfide-isomerase A3	473	8	24.95%	4−7	−1.42
2444	Q6AYU3	DnaJ homologue subfamily B member 6	100	2	11.20%	6−9	−1.49
		Protein synthesis					
335	Q8BHN3	Neutral alpha-glucosidase AB precursor	310	7	9.64%	4−7	1.3
1662	P04182	ornithine aminotransferase	356	8	28.47%	4−7	1.42
2168	P57776	eukaryotic translation elongation factor 1 delta	223	5	30.25%	4−7	−1.74
2264*	P57776	eukaryotic translation elongation factor 1 delta	223	5	30.25%	4−7	−1.4
2563	Q5XI72	eukaryotic translation initiation factor 4H	116	2	12.50%	4−7	−1.41
		Degradation					
317	Q5U300	Ubiquitin-activating enzyme E1	81	2	3.12%	4−7	−1.31
522	P46462	Valosin-containing protein	312	8	14.27%	4−7	−1.13
1702	O35987	NSFL1 (p97) cofactor	396	5	22.43%	4−7	−1.36
1861	Q3B7D1	Ubiquitin-conjugating enzyme E2 Z	178	4	16.29%	4−7	1.36
1878	Q9R0P3	*S*-formylglutathione hydrolase	243	4	28.37%	6−9	1.31
1929	Q3B7D1	Ubiquitin-conjugating enzyme E2 Z	45	1	2.53%	4−7	−1.15
2070	Q8WTY4	Anamorsin (Cytokine-induced apoptosis inhibitor 1)	232	3	15.53%	4−7	−1.32
2438	P55213	caspase 3	78	2	10.47%	4−7	1.21
2712	P60901	Proteasome subunit alpha type-6	509	8	49.19%	4−7	1.3
		Transport					
522	P46462	Valosin-containing protein	190	5	8.68%	4−7	−1.13
528	P46462	Valosin-containing protein	596	9	15.51%	4−7	−1.21

dx.doi.org/10.1021/pr101290n |*J. Proteome Res.* 2011, 10, 3372–3385

Table 1. Continued

spot no	Swiss-Prot ID	protein	ion score	peptides matched above identity threshold	percentage sequence coverage	pH range	fold regulation
2464	Q4QQV8	Charged multivesicular body protein 5	173	2	17.35%	4–7	−1.49
2479	Q66HR2	microtubule-associated protein, RP/EB family, member 1	170	4	25.00%	4–7	−1.62
		Oxidative stress					
1998*	P81155	Voltage-dependent anion-selective channel protein 2	115	2	15.25%	4–7	−1.42
2264*	Q920J4	Thioredoxin-like protein 1	98	2	12.46%	4–7	−1.4
2603	Q63716	Peroxiredoxin-1	79	2	12.56%	6–9	1.32
		Cell adhesion and proliferation					
356	Q64727	Vinculin	41	1	1.59%	4–7	−1.09
564	P15170	G1 to S phase transition protein 1 homologue	87	2	5.01%	4–7	−1.15
659	Q62871	Cytoplasmic dynein 1 intermediate chain 2	28	1	4.07%	4–7	−1.22
1398	P81377	cAMP-dependent protein kinase type I-beta regulatory subunit	368	5	21.00%	4–7	−1.12
2479	Q66HR2	microtubule-associated protein, RP/EB family, member 1	170	4	25.00%	4–7	−1.62
		Structural					
664	Q3KR86	Mitochondrial inner membrane protein	340	4	9.85%	4–7	−1.16
843	P48679	Lamin	48	1	2.41%	4–7	−1.41
1076	Q5RKI0	WD repeat protein 1	394	7	22.61%	4–7	−1.5
1209*	P21807	Peripherin	352	5	17.52%	4–7	−1.25
1283	P99024	tubulin, beta 5	441	8	26.80%	4–7	1.38
1849	Q5RJR2	Twinfilin-1	76	2	7.43%	4–7	1.19
2294	Q9D1E6	Tubulin-folding cofactor B	244	4	22.95%	4–7	−1.2
		Transcription and signaling					
564	P15170	G1 to S phase transition protein 1 homologue	87	2	5.01%	4–7	−1.15
1274	P61980	Heterogeneous nuclear ribonucleoprotein K	157	3	11.02%	4–7	−1.5
1407	Q8VHV7	Heterogeneous nuclear ribonucleoprotein H	292	5	20.49%	4–7	−1.18
1497	P09456	protein kinase, cAMP dependent regulatory, type I, alpha	446	8	37.01%	4–7	−1.2
1727	Q6URK4	heterogeneous nuclear ribonucleoprotein A3 isoform a	212	3	15.57%	6–9	1.43
2043	Q9Z204	Heterogeneous nuclear ribonucleoproteins C1/C2	165	3	12.14%	4–7	−1.65
2479	Q66HR2	microtubule-associated protein, RP/EB family, member 1	170	5	25.00%	4–7	−1.62
		Unknown					
2433	Q5I0D1	Glyoxalase domain-containing protein 4	100	2	9.06%	4–7	1.35

[a] Swiss-Prot accession number, protein name, ion score, number of identified peptide sequences above identity threshold, percentage sequence coverage, pH range and fold regulation of the proteins modified by oleate. Additional mass spectrometric information of the individual peptide sequences is shown in Supplementary Table 1 (Supporting Information). In case the identification only relies on a single peptide, the associated MS/MS spectrum is shown in the Supporting Information. In case more than one protein is present in a single spot, the different names/accession numbers are reported and indicated with an asterix (*).

Determination of ROS

Levels of cellular oxidative stress were measured using the fluorescent probe 2′,7′-dichlorofluorescein diacetate (DCFDA; Invitrogen). INS-1E cells were loaded for 30 min in the presence of 10 μM DCFDA at 37 °C. The formation of the fluorescent product DCF was determined by FACS analysis using a Gallios flow cytometer (Beckman Coulter, Brea, CA, USA) and Kaluza software (Beckman Coulter).

Determination of Intracellular ATP Levels

Intracellular ATP levels of INS-1E cells were measured using the ATPlite Luminescence assay system (Perkin-Elmer, Zaventem, Belgium) and normalized to total DNA content.

Quantitative RT-PCR

Total RNA from INS-1E cells was isolated by using the High Pure RNA Isolation kit (Roche Diagnostics). The qRT-PCR

Table 2. List of High Glucose + Oleate-Modified Proteins[a]

spot no	Swiss-Prot ID	protein	ion score	peptides matched above identity threshold	percentage sequence coverage	pH range	fold regulation
		Metabolism					
26	P16638	ATP-citrate synthase	29	1	1.45%	6−9	1.62
28	P16638	ATP-citrate synthase	28	1	1.45%	6−9	1.48
29	P16638	ATP-citrate synthase	35	1	1.45%	6−9	1.59
295	P11980	M2 pyruvate kinase	37	1	3.58%	6−9	−1.28
306	P11980	M2 pyruvate kinase	458	7	22.22%	6−9	1.34
372	P15999	ATP synthase subunit alpha	546	8	28.21%	6−9	1.27
373	P15999	ATP synthase subunit alpha	91	2	6.51%	6−9	1.23
391	P10860	glutamate dehydrogenase 1	442	7	24.19%	6−9	−1.53
398	P10860	glutamate dehydrogenase 1	506	8	24.37%	6−9	−1.34
400	P15999	ATP synthase subunit alpha	813	13	40.87%	6−9	−1.18
401	P15999	ATP synthase subunit alpha	489	8	21.88%	6−9	−1.28
407	P15999	ATP synthase subunit alpha	671	10	37.43%	6−9	−1.21
430	Q9DBF1	semialdehyde dehydrogenase	88	2	7.42%	6−9	−1.34
546	P25809	Creatine kinase, ubiquitous mitochondrial precursor	155	3	15.07%	6−9	1.51
552	P16617	phosphoglycerate kinase	92	2	11.99%	6−9	−1.26
553	P16617	phosphoglycerate kinase	324	5	25.90%	6−9	−1.2
576	P16617	phosphoglycerate kinase	207	3	17.03%	6−9	−1.71
658	P04797	Glyceraldehyde-3-phosphate dehydrogenase	84	2	10.81%	6−9	1.72
931	P08461	Pyruvate dehydrogenase complex, E2 component	149	3	11.39%	4−7	2.07
995	P08009	glutathione *S*-transferase	467	7	53.21%	6−9	1.64
1147	P19804	Nucleoside diphosphate kinase B	210	6	72.37%	6−9	1.67
1541	P04764	enolase A	219	6	26.04%	4−7	1.57
1579	P04764	enolase A	507	9	44.01%	4−7	1.4
1601	P04764	enolase A	98	2	9.45%	4−7	−1.16
1795	P12007	Isovaleryl-CoA dehydrogenase, mitochondrial	32	1	4.25%	4−7	−1.27
2125	O35077	Glycerol-3-phosphate dehydrogenase	185	3	13.75%	4−7	1.59
2493	P67779	Prohibitin	665	7	42.65%	4−7	−1.16
		Protein folding					
104	Q63617	ORP150	1247	13	22.82%	4−7	−1.1
715	P06761	GRP78	234	4	12.39%	4−7	−1.27
1003	P48721	GRP75	225	6	12.81%	4−7	−1.48
1106	P06761	GRP78	154	3	9.48%	4−7	−1.73
1146	P18418	Calreticulin	452	6	18.27%	4−7	−1.33
1274	Q9QVC8	FK506-binding protein 4	251	5	20.96%	4−7	1.56
1507	Q63081	Protein disulfide-isomerase A6	353	6	28.41%	4−7	1.17
3405	P11598	Protein disulfide-isomerase A3	38	1	2.77%	4−7	−1.26
		Protein synthesis					
70	P05197	eukaryotic translation elongation factor 2	598	9	17.48%	6−9	1.39
1037	P28841	Prohormone convertase 2	152	3	9.11%	4−7	−1.48
1059	P28841	Prohormone convertase 2	215	5	14.44%	4−7	−1.52
1081	P28841	Prohormone convertase 2	166	3	8.32%	4−7	−1.7
1342	P15087	Carboxypeptidase E	136	3	12.18%	4−7	−1.24
1764	Q5XIP1	Protein pelota homologue	119	3	15.32%	4−7	−1.38
		Degradation					
808	Q9Z2L0	voltage-dependent anion channel 1	506	8	62.19%	6−9	−1.45
815	Q9Z2L0	voltage-dependent anion channel 1	630	8	61.13%	6−9	−1.7
858	Q9Z2L0	voltage-dependent anion channel 1	450	5	36.40%	6−9	−1.85

Table 2. Continued

spot no	Swiss-Prot ID	protein	ion score	peptides matched above identity threshold	percentage sequence coverage	pH range	fold regulation
1147	P19804	Nucleoside diphosphate kinase B	210	6	71.71%	6−9	1.67
1238	Q4KMA2	UV excision repair protein RAD23 homologue B	135	3	9.40%	4−7	−1.43
1286	Q9JMJ4	Pre-mRNA-processing factor 19	240	6	25.40%	4−7	1.22
2737	P34064	Proteasome subunit alpha type-5	53	1	8.71%	4−7	−1.18
		Transport					
769	P52944	PDZ and LIM domain protein 1	365	5	36.70%	6−9	1.53
808	Q9Z2L0	voltage-dependent anion channel 1	506	8	62.19%	6−9	−1.45
815	Q9Z2L0	voltage-dependent anion channel 1	630	8	61.13%	6−9	−1.7
858	Q9Z2L0	voltage-dependent anion channel 1	450	5	36.40%	6−9	−1.85
		Oxidative stress					
808	Q9Z2L0	voltage-dependent anion channel 1	506	8	62.19%	6−9	−1.45
815	Q9Z2L0	voltage-dependent anion channel 1	630	8	61.13%	6−9	−1.7
858	Q9Z2L0	voltage-dependent anion channel 1	450	5	36.40%	6−9	−1.85
995	P08009	glutathione *S*-transferase, mu type 3	467	7	53.21%	6−9	1.64
2125	O35077	Glycerol-3-phosphate dehydrogenase	185	3	13.75%	4−7	1.59
		Cell adhesion and proliferation					
1764	Q5XIP1	Protein pelota homologue	119	3	15.32%	4−7	−1.38
		Structural					
172	O35303−3	dynamin-like protein DLP1 isoform DLP1−37	58	2	4.90%	6−9	−1.23
1044	P47942	Dihydropyrimidinase-related protein 2	31	1	4.20%	4−7	−1.54
1462	Q4V7C7	Actin-related protein 3	40	1	3.59%	4−7	1.62
		Transcription and signaling					
1286	Q9JMJ4	Pre-mRNA-processing factor 19	240	6	25.40%	4−7	1.22
1475	Q71UF4	Histone-binding protein RBBP7	91	2	13.65%	4−7	−1.22
1619	P29315	Ribonuclease inhibitor	282	4	12.72%	4−7	−1.14
1955	Q5XIG8	Serine-threonine kinase receptor-associated protein	37	1	4.86%	4−7	−1.36

[a] Swiss-Prot accession number, protein name, ion score, number of identified peptide sequences above identity threshold, percentage sequence coverage, pH range and fold regulation of the proteins modified by glucose + oleate. Additional mass spectrometric information of the individual peptide sequences is shown in Supplementary Table 2 (Supporting Information). In case the identification only relies on a single peptide, the associated MS/MS spectrum is shown in the Supporting Information.

amplification reaction was performed in a volume of 10 μL, containing 0.8 μL forward and reverse primers, 5 μL Fast SYBR Green Master Mix (Applied Biosystems) and 0.2 μL cDNA. The samples were assayed on an ABI-prism 7500 Fast (Applied Biosystems). The expression level of the gene of interest was normalized and corrected for the expression of hypoxanthine-guanine phosphoribosyltransferase (HPRT), which was not influenced by the experimental conditions. Correction for differences in efficiencies between gene of interest and housekeeping gene was done by the Pfaffl method.[26] The specific primer sequences for PC2 were: FW: 5′- AAGACGCAGCCTACATCACA-3′ and RV: 5′- TCTCTTTTTACGGTCAAATCCTTC-3′ and for HPRT FW: 5′-GTCAACGGGGGACATAAAAG-3′ and RV: 5′-GCTTGACCAAGGAAAGCAAA-3′.

Statistical Analysis

All data are presented as the means ± SEM. For all experiments, comparisons were performed by two-sided unpaired *t* test and a P value < 0.05 was considered statistically significant. For the proteomic analysis, a cutoff value of ±1.1 for the fold regulation was set.

RESULTS

Oleate-Induced INS-1E Cell Dysfunction and Apoptosis

Exposure of INS-1E cells to 0.5 mM oleate for 24 h induced beta cell dysfunction as shown by loss of GSIS: control cells almost doubled insulin secretion when glucose was raised from 3 to 30 mM, but no increase was seen in oleate-treated cells. Basal insulin secretion was not different. The combination of oleate and high glucose decreased basal and glucose-stimulated insulin secretion (Figure 1A). Oleate-exposed cells had lower total insulin content, which was further decreased in combination with high glucose (Figure 1B). Oleate also led to a mild increase in apoptosis (P < 0.05), that was amplified in combination with high glucose (Figure 2). No difference was observed in terms of necrosis.

Oleate-Induced Alterations in Protein Expression: 2D-DIGE and Protein Identification

The proteomic profile of INS-1E cells exposed for 24 h to oleate was determined using the 2D-DIGE technique. 87 spots were observed as differentially expressed ($P < 0.05$), when combining the results from the pH 4−7 and pH 6−9 2D gels. Of these differentially expressed spots, we were able to unambiguously identify 53 spots by MALDI-TOF/TOF, corresponding to an overall identification rate of 61% (Figure 3A). Several molecular pathways, such as transcription, translation, protein folding, degradation and intracellular transport were altered by exposure to oleate. The complete list of oleate-modified proteins, grouped in functional classes according to the gene ontology classification, is shown in Table 1. The table includes information on the Swiss-Prot accession number, ion score, number of identified peptide sequences above identity threshold, pH range and fold regulation. Additional mass spectrometric information of the individual peptide sequences, as well as the false discovery rate based on a decoy base, is shown in Supplementary Table 1 (Supporting Information). In case the identification only relies on a single peptide, the associated MS/MS spectrum is also shown in the supplementary data.

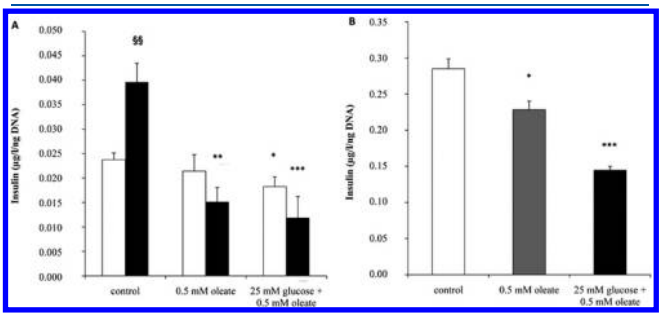

Figure 1. Oleate impairs GSIS and decreases insulin content. (A) After a 24 h exposure to 11 mM glucose (control) or 0.5 mM oleate, combined or not with 25 mM glucose, INS-1E cells were incubated at low (3 mM glucose − white bars) or high (30 mM glucose − black bars) glucose for 1 h. Secretion of insulin to the medium was determined and normalized for total DNA content. Results are means ± SEM ($n = 4$). *$P < 0.05$; ** $P < 0.01$; *** $P < 0.001$ versus control; §§ $P < 0.01$ versus 3 mM glucose. (B) Insulin content was determined after a 24 h exposure of INS-1E cells to 11 mM glucose (control) or 0.5 mM oleate, combined or not with 25 mM glucose and normalized for total DNA content. Results are means ± SEM ($n = 4$). *$P < 0.05$; *** $P < 0.001$ versus control.

Alterations in Metabolic Proteins

Glycolytic enzymes were either up- (phosphoglycerate kinase) or downregulated (enolase). In the Krebs cycle, isocitrate dehydrogenase and glutamate dehydrogenase were upregulated.

Alterations in Protein Folding

Proteomic analysis revealed a downregulation of major chaperone proteins. Heat shock protein 70 kDA (HSP70) 8, glucose-regulated protein 78 kDa (GRP78, also known as BiP or HSPA5), 60 kDA HSP, protein disulfide isomerase A3 and DNAJ homologue protein, which acts as a cochaperone of HSP70, were downregulated by oleate.

Alterations in Transcription and Translation Related Proteins

Exposure to oleate induced the downregulation of 3 different heterogeneous nuclear ribonucleoproteins (HNRP) (K; H and C1/C2) that bind to and stabilize pre-mRNA and play important roles in mRNA processing and transport. The changes in RNA handling were also accompanied by a downregulation of eukaryotic initiation factor (eIF)4H and by a downregulation of two isoforms related to eukaryotic elongation factor (eEF)1δ.

Alterations in Degradation

Several proteins involved in the ubiquitin-associated degradation pathway were downregulated in INS-1E cells exposed to oleate. Enzymes involved in the ubiquitination (ubiquitin-activating enzyme E1 and ubiquitin conjugating enzyme E2Z) were downregulated by oleate. Valosin-containing protein (VCP) and NSFL1 cofactor that play important roles in the transfer of misfolded proteins out of the ER to the proteasome were downregulated. Additionally, VCP also regulates E3 ubiquitin-protein ligase activity.[27]

Alterations in Intracellular Transport and Vesicle Docking

Dynein 1 intermediate chain, which mediates the binding of dynein to dynactin and the retrograde motility of vesicles and organelles along microtubules, as well as microtubule-associated protein that also interacts with dynein, were downregulated. Two isoforms of VCP that associate with clathrin and play an important role in general vesicle-associated transport were also downregulated by oleate.

Alterations in Protein Expression Induced by High Glucose and Oleate: 2D-DIGE and Protein Identification

The proteomic profile of INS-1E cells exposed for 24 h to oleate, combined with 25 mM glucose, was determined using the 2D-DIGE technique. Seventy-nine spots were observed as

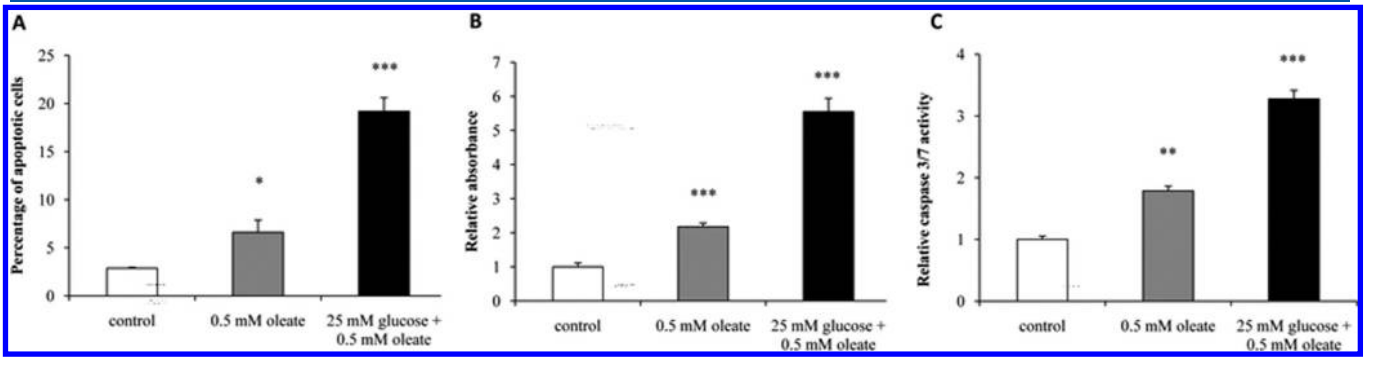

Figure 2. Apoptosis induced by oleate, combined or not with high glucose.
INS-1E cells were exposed to 0.5 mM oleate, combined or not with 25 mM glucose for 24 h. Apoptosis of INS-1E cells was assessed by (A) microscopy, (B) DNA fragmentation and (C) caspase 3/7 activity. Data are shown as mean ± SEM ($n = 4$). * $P < 0.05$; ** $P < 0.01$; *** $P < 0.001$ versus control.

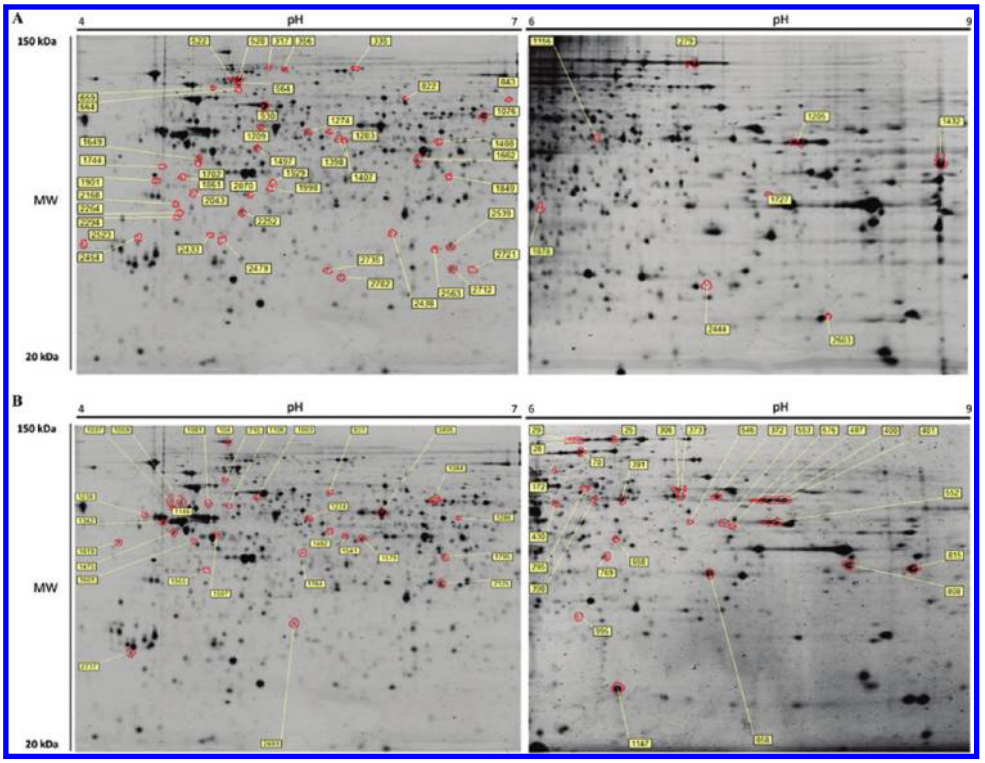

Figure 3. Overview of the gel images and the differentially expressed proteins by oleate alone and by the combination of high glucose and oleate. (A) Grayscale images of 2D-DIGE in the pH range 4−7 and 6−9 of INS-1E cells, exposed to oleate alone. Of a total of 87 spots, 53 could unambiguously be identified by MALDI-TOF analysis using Peptide Mass Fingerprint (PMF) and fragmentation (MS/MS) of the most intense peaks of PMF and these spots are highlighted (n = 4). (B) Grayscale images of 2D-DIGE in the pH range 4−7 and 6−9 of INS-1E cells, exposed to the combination of high glucose and oleate. Of a total of 79 spots, 54 could unambiguously be identified by MALDI-TOF analysis using Peptide Mass Fingerprint (PMF) and fragmentation (MS/MS) of the most intense peaks of PMF and these spots are highlighted (n = 4).

differentially expressed ($P < 0.05$), when combining the results from the pH 4−7 and pH 6−9 2D gels. Of these differentially expressed spots, we were able to unambiguously identify 54 spots by MALDI-TOF/TOF, corresponding to an overall identification rate of 68% (Figure 3B). Mainly proteins involved in metabolism, protein synthesis and folding, degradation and oxidative stress were altered. The complete list of identified proteins grouped in functional classes according to gene ontology is shown in Table 2. The table includes information on the Swiss-Prot accession number, ion score, number of identified peptide sequences above identity threshold, pH range and fold regulation. Additional mass spectrometric information of the individual peptide sequences, as well as the false discovery rate based on a decoy base, is shown in Supplementary Table 2 (Supporting Information). In case the identification only relies on a single peptide, the associated MS/MS spectrum is also shown in the supplementary data.

Combination of High Glucose and Oleate Increases the Import of Acetyl-CoA in the Krebs Cycle, Which Is Not Coupled to ATP Production

The E2 component of the pyruvate dehydrogenase complex, the key enzyme regulating the conversion of pyruvate to acetyl-CoA that subsequently can be used in the Krebs cycle, was upregulated. The increased input of acetyl-CoA in the Krebs cycle did not seem to be coupled to the production of ATP by the mitochondrial respiratory chain, as three isoforms of ATP synthase alpha, a key enzyme for ATP production, were downregulated by the exposure to glucose and oleate (Figure 4). ATP-citrate synthase, a crucial enzyme for the synthesis of cytosolic acetyl-CoA and *de novo* lipid synthesis, was respresented by 3 different spots, all being upregulated by the combination of glucose and oleate.

Alterations in Chaperone Levels

Proteomic analysis of oleate + high glucose-treated INS-1E cells revealed a downregulation of several chaperones, such as ORP150, GRP75, calreticulin, PDIA3 and two isoforms of GRP78.

Generation of ROS

The combination of glucose and oleate induced glutathione S-transferase, an important detoxifying enzyme for environmental toxins and ROS. Three different isoforms of voltage-dependent anion channel (VDAC) 1 were downregulated. This highly conserved mitochondrial protein passes ions and metabolites across the mitochondrial outer membrane and protects against ROS produced by the respiratory chain. Glucose and oleate also induced an upregulation of glycerol-3-phosphate dehydrogenase that can convert dihydroxyacetone phosphate into glycerol-3-phosphate, leading to increased DAG production with increased protein kinase C activation and ROS production as a consequence (Figure 4).

Impaired Processing of Pro-insulin to Insulin by Oleate

Prohormone convertase 2 and carboxypeptidase E, two essential enzymes in the maturation of insulin that cleave pro-insulin into insulin and C-peptide, were downregulated by high glucose + oleate. Three different isoforms of PC2 were decreased

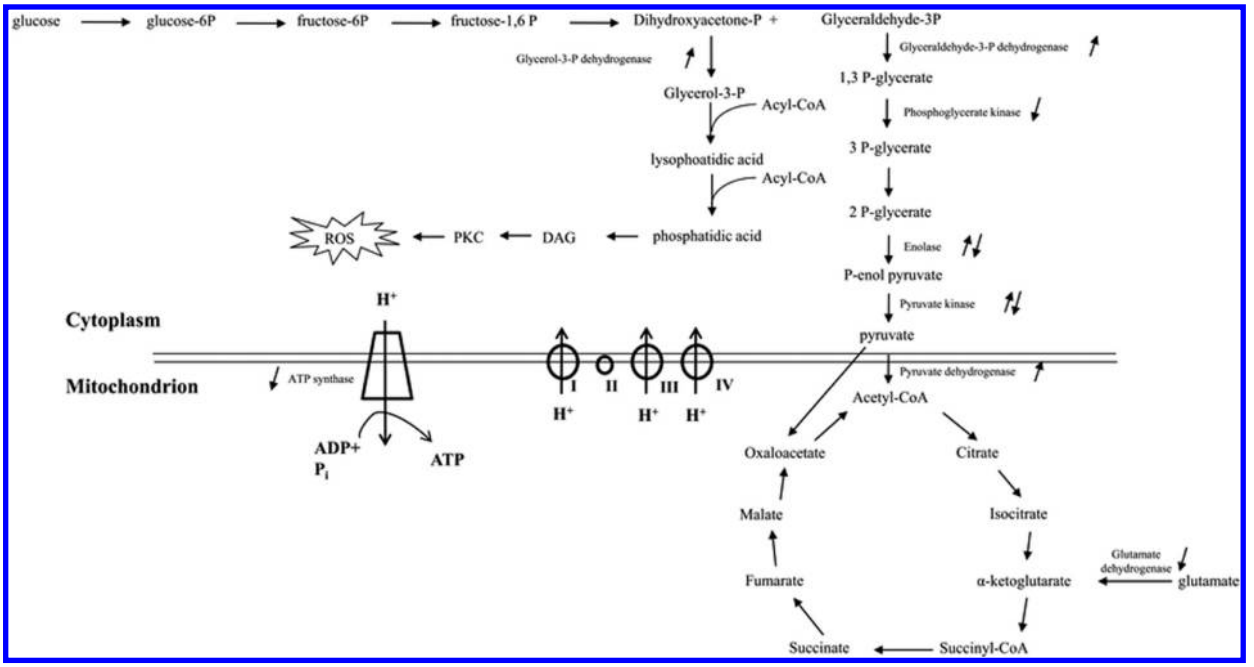

Figure 4. Schematic overview of the metabolic pathway, modulated by oleate in the presence of high glucose. The combination of glucose and oleate increased the entry of acetyl-CoA levels in the Krebs cycle, but this was not coupled to increased ATP production. Moreover, glycerol-3-phosphate dehydrogenase that can shunt excess of glucose into detrimental pathways was also upregulated. Arrows indicate the up- or downregulation of proteins involved in this pathway, as revealed from the 2D-DIGE analysis.

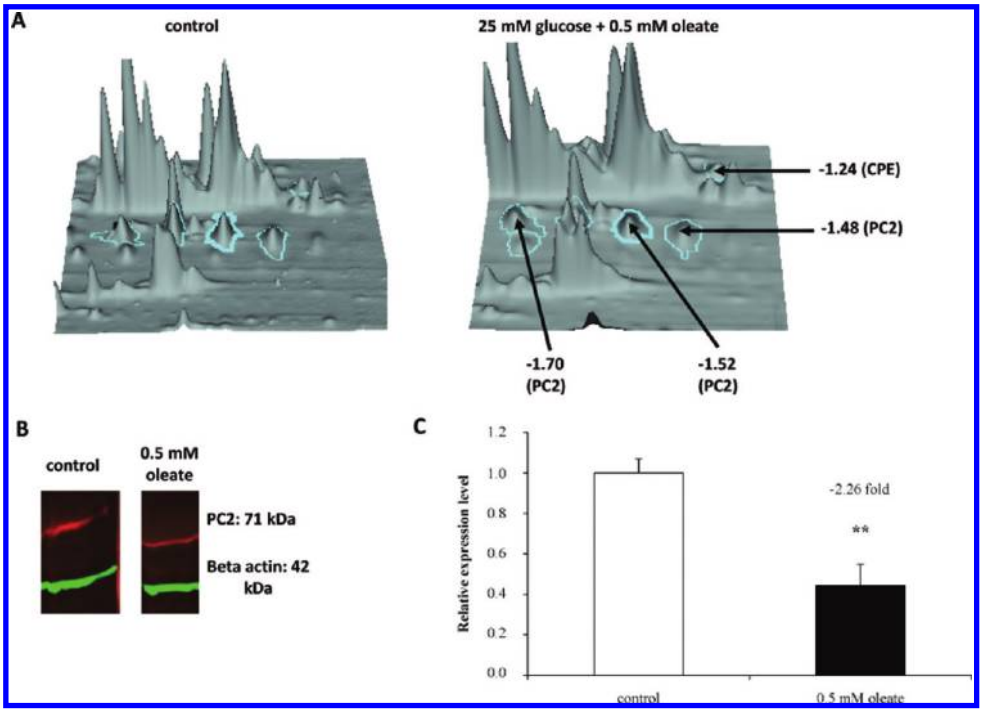

Figure 5. Oleate, combined or not with high glucose, decreases PC2 and CPE expression. (A) Three-dimensional view, showing the downregulation of PC2 and CPE by glucose and oleate compared to control. (B−C) Total PC2 protein levels of INS-1E cells treated with 11 mM glucose (control) or 0.5 mM oleate for 24 h. A representative image of the Western blot is shown (B) and the quantitative data (normalized to beta actin) (C). Results are means ± SEM ($n = 4$) ** $P < 0.01$ versus control.

by −1.48 to −1.70 (Figure 5A). Additionally, oleate-treated INS-1E cells also showed a 2.26 fold lower total PC2 protein expression level (Figure 5B−C).

Functional Assays Confirming Proteomic Results

Intracellular ATP Content. The combination of oleate and high glucose induced a downregulation of ATP synthase alpha

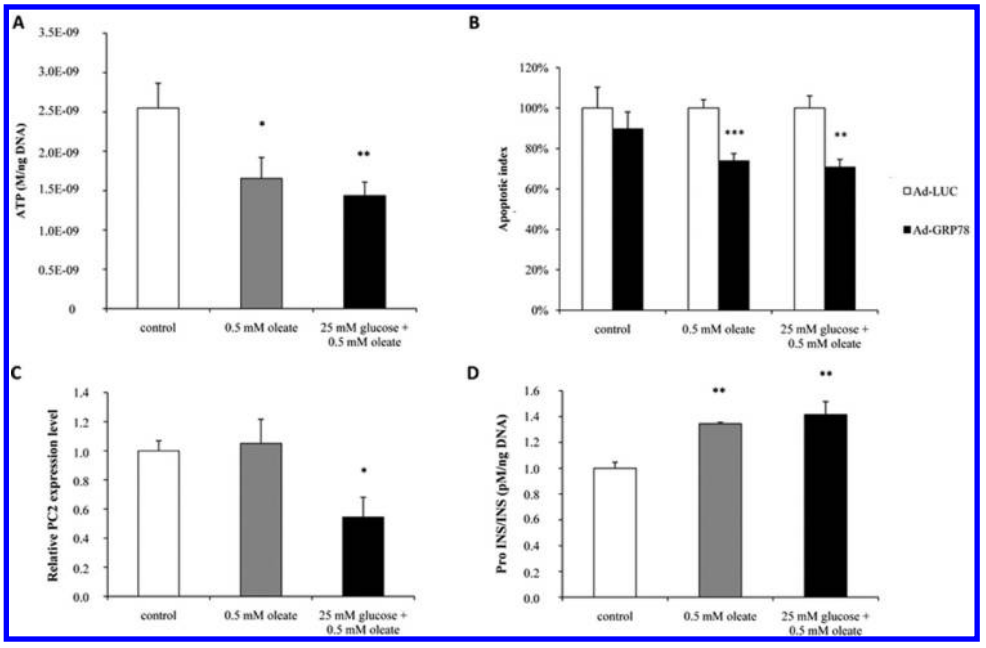

Figure 6. Functional assays confirming proteomic results. (A) Oleate decreases intracellular ATP content: after 24 h of exposure to 11 mM glucose (control) or 0.5 mM oleate, combined or not with 25 mM glucose, total intracellular ATP content was determined and normalized for total DNA content. Results are means ± SEM ($n = 4$). *$P < 0.05$; ** $P < 0.01$ versus control. (B) Replenishment of GRP78 protein protects INS-1E cells against oleate-induced cell death: INS-1E cells were incubated in medium containing Ad-LUC or Ad-GRP78 at a multiplicity of infection of 1 for 2 h at 37 °C. After a 24 h exposure of infected cells to the indicated stimuli, protection against apoptosis was determined. Results are means ± SEM ($n = 6$). ** $P < 0.01$; *** $P < 0.001$ versus Ad-LUC. (C) Relative PC2 mRNA expression level normalized to the stable housekeeping gene HPRT in INS-1E cells, exposed to 11 mM glucose (control) or 0.5 mM oleate, combined or not with 25 mM glucose. Results are means ± SEM ($n = 4$). * $P < 0.05$ versus control. (D) After 24 h of exposure to 11 mM glucose (control) or 0.5 mM oleate, combined or not with 25 mM glucose, total pro-insulin and insulin content were determined, normalized for total DNA content, and afterward the ratio was calculated. Results are means ± SEM ($n = 4$). **$P < 0.01$ versus control.

and beta, an observation corroborated by a decreased total ATP content by 44% ($P < 0.01$). Additionally, oleate by itself also downregulated ATP content by 35% (Figure 6A) in keeping with previous findings.[28]

GRP78 Overexpression Protects INS-1E Cells against (Glucose +) Oleate-Induced Cell Death. As the GRP78 chaperone was downregulated by oleate and the combination of glucose and oleate, the consequence of this chaperone depletion was evaluated by replenishment of GRP78 protein using an adenoviral GRP78 expression vector. The increase in GRP78 protein protected INS-1E cells from oleate- and high glucose + oleate-induced apoptosis (Figure 6B).

Intracellular ROS Levels. A 24 h exposure of INS-1E cells to oleate decreased intracellular ROS levels by 11.4 ± 1.7% ($P < 0.001$ versus control; $n = 11$), whereas the combination of oleate and high glucose increased intracellular ROS levels by 17.4 ± 2.8% ($P < 0.001$ versus control, $n = 11$), confirming the proteomic results.

PC2 mRNA Expression and Pro-insulin to Insulin Ratio. In line with a downregulation of PC2 at the protein level, an inhibitory effect was also observed at the PC2 mRNA level for glucose + oleate but not for oleate alone (Figure 6C). We next examined whether the decrease in this enzyme affected the conversion of pro-insulin to insulin. The ratio of pro-insulin to insulin increased by 35% following oleate treatment at normal and high glucose concentrations (Figure 6D).

DISCUSSION

In this study, we describe the proteome changes, induced by the unsaturated FFA oleate, in the presence of normal or high glucose concentrations. In line with previous reports, exposure of INS-1E cells to oleate induced mild apoptosis,[11,29] and this was amplified by high glucose.[12] Oleate-exposed INS-1E cells were also dysfunctional, having impaired GSIS and decreased insulin content, even further aggravated by the addition of high glucose. These data are comparable with oleate-induced dysfunction in pancreatic islets,[15,30] confirming that the INS-1E cell line is a valid model for our proteomic study of lipotoxic beta cell dysfunction.

We did not detect major changes in glycolysis and Krebs cycle enzymes after exposure to oleate alone, which is in line with previous observations that oleate did not affect glucose usage and contents of glycolytic enzymes.[31] Oleate induced an upregulation of NADH dehydrogenase and ATP synthase, the first and last enzyme of the mitochondrial electron transport chain. However, this upregulation did not lead to elevated ATP content. As intracellular ATP levels are a critical link between mitochondrial metabolism and insulin secretion through the closure of ATP-dependent K^+ channels and depolarization of the beta cell membrane,[32] the lowered ATP content can contribute to the impaired GSIS. Intracellular ROS levels were also decreased by oleate. As it has been demonstrated in INS-1 cells and mouse islets that physiological levels of ROS are required for normal beta cell function,[33] lower intracellular ROS levels can also contribute to the oleate-induced dysfunction.

The metabolic profile changed considerably when INS-1E cells were exposed to the combination of oleate and high glucose. There was an upregulation of the E2 component (i.e., dihydrolipoamide acetyltransferase) of the pyruvate dehydrogenase complex. As this component is responsible for the transfer of the acetyl group to coenzyme A, it plays an important role in the pyruvate dehydrogenase complex, which is responsible for the irreversible oxidative decarboxylation of pyruvate to acetyl CoA. The PHD complex is a rate-limiting enzyme in the control of the import of acetyl-CoA into the mitochondria and Krebs cycle. Three different isoforms related to ATP citrate synthase were upregulated, suggestive for cataplerosis as this enzyme is able to convert cytosolic citrate into oxaloacetate and acetyl-CoA, which can be converted into malonyl-CoA by ACC. Malonyl-CoA can inhibit CPT-I, causing a metabolic switch from fat to glucose oxidation with subsequent formation of long-chain fatty acids. This process is accompanied by the production of metabolites, which can interfere with insulin gene expression, synthesis and secretion.[15,34] A downregulation of ATP citrate synthase has been associated with apoptosis after exposure of MIN6 cells to glucose + palmitate. In this view, the observed upregulation by glucose + oleate can contribute to the milder apoptosis induced by the combination of glucose and oleate as compared to glucose and palmitate.[35] When high levels of both glucose and FFA are available as an energy source, excess glucose is shunted toward nonclassic metabolic pathways. In this context, we detected an upregulation of glycerol-3-phosphate dehydrogenase, an essential enzyme in the shunting of dihydroxyacetone phosphate toward *de novo* synthesis of diacylglycerol that in turn activates protein kinase C. PKC activation is associated with the generation of several detrimental signaling molecules, such as TGF-β1, NF-κB, and ROS.[36]

The combination of high glucose and oleate downregulated three isoforms of ATP synthase alpha. These changes are suggestive for an impaired coupling between increased glucose metabolism and ATP production. This can result in a lower intracellular ATP content, which plays an important role in insulin secretion. The mitochondrial electron transport chain is a major source of intracellular ROS,[37] of which $O_2^{\cdot -}$ is transported by VDAC1 to the cytosol where it is detoxified.[38] The presently observed downregulation of three isoforms of VDAC1 can cause intramitochondrial accumulation of $O_2^{\cdot -}$[39] and elicit the opening of high conductance permeability transition pores in the mitochondrial inner membrane. These permeability transition pores will initiate the onset of the mitochondrial permeability transition with consequent mitochondrial depolarization, uncoupling of oxidative phosphorylation, mitochondrial swelling and activation of apoptotic pathways.[40] This is in keeping with the previous observations that oleate induces mitochondrial cytochrome c release.[10] UCP2 may dissipate the proton electrochemical gradient[41] and it has been demonstrated that FFA activate UCP2 uncoupling. These changes will blunt the rise in proton-motive force, which is essential for a proper GSIS.[41−43] We did not detect changes in UCP2 expression, but this may be a matter of technical limitations of the 2D-DIGE technique to detect low-abundant proteins.

Proteomic analysis revealed a downregulation of major chaperones and folding enzymes by oleate alone or the combination of high glucose and oleate. Because oleate induces a milder UPR compared to palmitate, most studies have not focused on the effects of oleate on chaperones. In one study, no change in GRP78 and PDI expression was detected by Western blotting.[11] This may be explained by the greater sensitivity of proteomics compared to Western blotting and the ability to differentiate between different isoforms. The upregulation of some isoforms and the downregulation of others may be missed by Western blotting, as was the case for PDI (present data). The downregulation of chaperones contributes to cellular dysfunction and beta cell death, as shown by our finding that GRP78 replenishment protected against (gluco)lipotoxic apoptosis.

Another important alteration induced by oleate alone was the downregulation of transcription and translation related proteins. Oleate decreased expression of three HNRPs. These are highly abundant nuclear RNA-binding proteins that bind to the nascent mRNA transcript during transcriptional elongation and play central roles in mRNA life cycle, including packaging, export and translation.[44] In other cell types the downregulation of HNRPs has been shown to increase apoptosis[45−47] and the knock-down of HNRP C1/C2 increased sensitivity to peroxide and various chemicals.[48] The HNRP effect on apoptosis occurs through alternative splicing of Bcl-2 family members,[49] the destabilization[50] or facilitated cap-independent translation of mRNAs, encoding members of the inhibitor of apoptosis protein family.[51] The decreased HNRP expression by oleate is likely to alter the machinery for RNA splicing, but it can also directly or indirectly influence cellular homeostasis, shifting the cells to dysfunction. In parallel, oleate downregulated key enzymes in translational activity (eIF-4H and eEF-1δ), which together with the previously reported eIF2α phosphorylation,[11] may explain the decrease in translation.[29] Prolonged translational inhibition contributes in the activation of pro-apoptotic pathways.

The proteomic analysis also demonstrates that oleate alone regulates proteins of the ubiquitin proteasome pathway. Oleate downregulated the E1 and E2 enzymes responsible for the activation and conjugation of ubiquitin to misfolded proteins. Oleate also lowered expression of VCP and NSFL1 cofactor, two proteins that are part of a ternary complex with a pivotal role in targeting misfolded proteins in the ER toward degradation and in the regulation of ubiquitin ligase activity.[27] Unsaturated FFA can inhibit protein degradation at a postubiquitination level by interfering with the VCP complex.[52] The impaired ubiquitin-related degradation and diminished ER export to the proteasome can result in the accumulation and aggregation of misfolded and unfolded proteins in the ER. The altered expression of PDI may affect pro-insulin folding. The aggregation can be further promoted by the downregulation of 70 kDa HSP, which plays an essential role in the solubilization and elimination of aggregates.[53]

Oleate also has detrimental effects on the processing of insulin. CPE and three isoforms of PC2 were downregulated by combined exposure of high glucose and oleate. We did not detect a significant change by oleate alone in the proteomic analysis. A technical limitation may explain the absence of PC2 regulation by oleate: given that PC2 is represented by a horizontal train of spots, variability in the separation of PC2 in the 4 independent experiments might have affected its detection. This is supported by the marked downregulation of total PC2 protein by oleate, both at 11 or 25 mM glucose, as observed by Western blotting. These changes affected pro-insulin processing, as suggested by the increased pro-insulin to insulin content. The downregulation of PC2 can also hamper the processing of proIAPP, which contributes to amyloid formation and beta cell dysfunction.[54]

Interference with vesicle transport and budding is another level at which oleate potentially contributes to impair GSIS. Oleate downregulated dynein 1 intermediate chain, which

mediates the binding of dynein to dynactin and the retrograde motility of vesicles and organelles along microtubules.[55] In addition, microtubule-associated protein RP/EB1 that is involved in microtubule polymerization,[56] was also downregulated by oleate. Vesicle budding can also be hampered as two isoforms of VCP protein were downregulated by oleate. It has been shown that VCP associates with clathrin, perhaps serving as a chaperone in the assembly and disassembly of the clathrin coat.[57,58]

In conclusion, we confirm that unsaturated fatty acids, like oleate, can contribute to beta cell dysfunction and death, described as (gluco)lipotoxicity. We have identified novel pathways that contribute to the oleate-induced beta cell dysfunction and apoptosis using a proteomic approach. Modifications in transcription, translation and pro-insulin folding and processing contribute to impair insulin biosynthesis. Ubiquitin-associated degradation and vesicle transport are inhibited, which can further cause beta cell dysfunction. Finally, the combination of oleate with high glucose worsens beta cell death by the generation of ROS and by promoting fatty acid synthesis, accompanied by the production of harmful side products.

■ ASSOCIATED CONTENT

Supporting Information

Supplementary tables and data. This material is available free of charge via the Internet at http://pubs.acs.org.

■ AUTHOR INFORMATION

Corresponding Author

*Lutgart Overbergh, Laboratory for Experimental Medicine and Endocrinology (LEGENDO), University Hospital Gasthuisberg, Herestraat 49, Catholic University of Leuven, Leuven, Belgium. Tel: +32 16 346163. Fax: +32 16 345970. E-mail: lut.overbergh@med.kuleuven.be.

■ ACKNOWLEDGMENT

This work was supported by the European Union (STREP SaveBeta no. 036,903 in the Framework Program 6 and Cooperation NAIMIT no. 241447 and Collaborative Project CEED3 in the Framework Program 7, the Catholic University of Leuven (GOA 2004/10 and 2009/10), the Flemish Research Foundation (FWO G.0552.06 and G.0649.08), the Belgium Program on Interuniversity Poles of Attraction initiated by the Belgian State (IUAP P5/17 and P6/40), a European Foundation for the Study of Diabetes EFSD/Lilly grant, the Centre of Excellence SymBioSys (Research Council K.U.Leuven EF/05/007) and an unrestricted educational grant from Merck Sharp & Dohme. C.M. was supported by a clinical research fellowship (FWO), and M.C. was supported by the Fonds National de la Recherche Scientifique (FNRS) - Fonds de la Recherche Scientifique Médicale (FRSM). The technical experience of Jos Depovere, Karin Schildermans, and Sandy Vandoninck is greatly appreciated.

■ ABBREVIATIONS

eEF, eukaryotic elongation factor; eIF, eukaryaotic initiation factor; ER, endoplasmic reticulum; FFA, free fatty acids; GRP75, 75 kDa glucose regulated protein; GRP78, 78 kDa glucose regulated protein; HNRP, heterogeneous nuclear ribonucleoprotein; HSP, heat shock protein; ORP150, 150 kDa oxygen-regulated protein; PC2, prohormone convertase 2; PDIA, protein disulfide isomerase; ROS, reactive oxygen species; T2D, type 2 diabetes; VDAC, voltage-dependent anion channel.

■ REFERENCES

(1) Butler, A. E.; Janson, J.; Bonner-Weir, S.; et al. Beta-cell deficit and increased beta-cell apoptosis in humans with type 2 diabetes. *Diabetes* **2003**, *52*, 102–110.

(2) Silveira, L. R.; Fiamoncini, J.; Hirabara, S. M.; et al. Updating the effects of fatty acids on skeletal muscle. *J. Cell Physiol.* **2008**, *217*, 1–12.

(3) Tilg, H.; Moschen, A. R. Adipocytokines: mediators linking adipose tissue, inflammation and immunity. *Nat. Rev. Immunol.* **2006**, *6*, 772–783.

(4) de Ferranti, S.; Mozaffarian, D. The perfect storm: obesity, adipocyte dysfunction, and metabolic consequences. *Clin. Chem.* **2008**, *54*, 945–955.

(5) Unger, R. H. Lipotoxicity in the pathogenesis of obesity-dependent NIDDM. Genetic and clinical implications. *Diabetes* **1995**, *44*, 863–870.

(6) Prentki, M.; Joly, E.; El-Assaad, W.; et al. Malonyl-CoA signaling, lipid partitioning, and glucolipotoxicity: role in beta-cell adaptation and failure in the etiology of diabetes. *Diabetes* **2002**, *51* (Suppl 3), S405–S413.

(7) Diakogiannaki, E.; Dhayal, S.; Childs, C. E.; et al. Mechanisms involved in the cytotoxic and cytoprotective actions of saturated versus monounsaturated long-chain fatty acids in pancreatic beta-cells. *J. Endocrinol.* **2007**, *194*, 283–291.

(8) Dhayal, S.; Welters, H. J.; Morgan, N. G. Structural requirements for the cytoprotective actions of mono-unsaturated fatty acids in the pancreatic beta-cell line, BRIN-BD11. *Br. J. Pharmacol.* **2008**, *153*, 1718–1727.

(9) Eitel, K.; Staiger, H.; Brendel, M. D.; et al. Different role of saturated and unsaturated fatty acids in beta-cell apoptosis. *Biochem. Biophys. Res. Commun.* **2002**, *299*, 853–856.

(10) Maestre, I.; Jordan, J.; Calvo, S.; et al. Mitochondrial dysfunction is involved in apoptosis induced by serum withdrawal and fatty acids in the beta-cell line INS-1. *Endocrinology* **2003**, *144*, 335–345.

(11) Karaskov, E.; Scott, C.; Zhang, L.; et al. Chronic palmitate but not oleate exposure induces endoplasmic reticulum stress, which may contribute to INS-1 pancreatic beta-cell apoptosis. *Endocrinology* **2006**, *147*, 3398–3407.

(12) Cunha, D. A.; Hekerman, P.; Ladriere, L.; et al. Initiation and execution of lipotoxic ER stress in pancreatic beta-cells. *J. Cell Sci.* **2008**, *121*, 2308–2318.

(13) Wang, Y.; Wang, P. Y.; Takashi, K. Chronic effects of different non-esterified fatty acids on pancreatic islets of rats. *Endocrine* **2006**, *29*, 169–173.

(14) Kudo, T.; Wu, J.; Ogawa, Y.; et al. Novel mechanism of chronic exposure of oleic acid-induced insulin release impairment in rat pancreatic beta-cells. *J. Pharmacol. Exp. Ther.* **2006**, *318*, 1203–1210.

(15) Olofsson, C. S.; Collins, S.; Bengtsson, M.; et al. Long-term exposure to glucose and lipids inhibits glucose-induced insulin secretion downstream of granule fusion with plasma membrane. *Diabetes* **2007**, *56*, 1888–1897.

(16) Collins, S. C.; Salehi, A.; Eliasson, L.; et al. Long-term exposure of mouse pancreatic islets to oleate or palmitate results in reduced glucose-induced somatostatin and oversecretion of glucagon. *Diabetologia* **2008**, *51*, 1689–1693.

(17) Busch, A. K.; Cordery, D.; Denyer, G. S.; et al. Expression profiling of palmitate- and oleate-regulated genes provides novel insights into the effects of chronic lipid exposure on pancreatic beta-cell function. *Diabetes* **2002**, *51*, 977–987.

(18) Ortsater, H.; Sundsten, T.; Lin, J. M.; et al. Evaluation of the SELDI-TOF MS technique for protein profiling of pancreatic islets exposed to glucose and oleate. *Proteomics* **2007**, *7*, 3105–3115.

(19) Merglen, A.; Theander, S.; Rubi, B.; et al. Glucose sensitivity and metabolism-secretion coupling studied during two-year continuous culture in INS-1E insulinoma cells. *Endocrinology* **2004**, *145*, 667–678.

(20) Asfari, M.; Janjic, D.; Meda, P.; et al. Establishment of 2-mercaptoethanol-dependent differentiated insulin-secreting cell lines. *Endocrinology* **1992**, *130*, 167–178.
(21) Hoorens, A.; Van de, C. M.; Kloppel, G.; et al. Glucose promotes survival of rat pancreatic beta cells by activating synthesis of proteins which suppress a constitutive apoptotic program. *J. Clin. Invest.* **1996**, *98*, 1568–1574.
(22) D'Hertog, W.; Overbergh, L.; Lage, K.; et al. Proteomics analysis of cytokine-induced dysfunction and death in insulin-producing INS-1E cells: new insights into the pathways involved. *Mol. Cell. Proteomics* **2007**, *6*, 2180–2199.
(23) D'Hertog, W.; Overbergh, L.; Lage, K.; et al. Proteomics analysis of cytokine-induced dysfunction and death in insulin-producing INS-1E cells: new insights into the pathways involved. *Mol. Cell. Proteomics* **2007**, *6*, 2180–2199.
(24) Altschul, S. F.; Madden, T. L.; Schaffer, A. A.; et al. Gapped BLAST and PSI-BLAST: a new generation of protein database search programs. *Nucleic Acids Res.* **1997**, *25*, 3389–3402.
(25) Hopcroft, D. W.; Mason, D. R.; Scott, R. S. Standardization of insulin secretion from pancreatic islets: validation of a DNA assay. *Horm. Metab. Res.* **1985**, *17*, 559–561.
(26) Pfaffl, M. W. A new mathematical model for relative quantification in real-time RT-PCR. *Nucleic Acids Res.* **2001**, *29*, e45.
(27) Ishigaki, S.; Hishikawa, N.; Niwa, J.; et al. Physical and functional interaction between Dorfin and Valosin-containing protein that are colocalized in ubiquitylated inclusions in neurodegenerative disorders. *J. Biol. Chem.* **2004**, *279*, 51376–51385.
(28) Frigerio, F.; Brun, T.; Bartley, C.; et al. Peroxisome proliferator-activated receptor alpha (PPARalpha) protects against oleate-induced INS-1E beta cell dysfunction by preserving carbohydrate metabolism. *Diabetologia* **2010**, *53*, 331–340.
(29) Cnop, M.; Ladriere, L.; Hekerman, P.; et al. Selective inhibition of eukaryotic translation initiation factor 2 alpha dephosphorylation potentiates fatty acid-induced endoplasmic reticulum stress and causes pancreatic beta-cell dysfunction and apoptosis. *J. Biol. Chem.* **2007**, *282*, 3989–3997.
(30) Oprescu, A. I.; Bikopoulos, G.; Naassan, A.; et al. Free fatty acid-induced reduction in glucose-stimulated insulin secretion: evidence for a role of oxidative stress in vitro and in vivo. *Diabetes* **2007**, *56*, 2927–2937.
(31) Segall, L.; Lameloise, N.; Assimacopoulos-Jeannet, F.; et al. Lipid rather than glucose metabolism is implicated in altered insulin secretion caused by oleate in INS-1 cells. *Am. J. Physiol.* **1999**, *277*, E521–E528.
(32) Rorsman, P.; Trube, G. Glucose dependent K+-channels in pancreatic beta-cells are regulated by intracellular ATP. *Pflugers Arch.* **1985**, *405*, 305–309.
(33) Pi, J.; Bai, Y.; Zhang, Q.; et al. Reactive oxygen species as a signal in glucose-stimulated insulin secretion. *Diabetes* **2007**, *56*, 1783–1791.
(34) Poitout, V.; Hagman, D.; Stein, R.; et al. Regulation of the insulin gene by glucose and fatty acids. *J. Nutr.* **2006**, *136*, 873–876.
(35) Chu, K. Y.; Lin, Y.; Hendel, A.; et al. ATP-citrate lyase reduction mediates palmitate-induced apoptosis in pancreatic beta-cells. *J. Biol. Chem.* **2010**, *285*, 32606–32615.
(36) Robertson, R. P.; Harmon, J.; Tran, P. O.; et al. Beta-cell glucose toxicity, lipotoxicity, and chronic oxidative stress in type 2 diabetes. *Diabetes* **2004**, *53* (Suppl 1), S119–S124.
(37) Cadenas, E.; Davies, K. J. Mitochondrial free radical generation, oxidative stress, and aging. *Free Radic. Biol. Med.* **2000**, *29*, 222–230.
(38) Han, D.; Antunes, F.; Canali, R.; et al. Voltage-dependent anion channels control the release of the superoxide anion from mitochondria to cytosol. *J. Biol. Chem.* **2003**, *278*, 5557–5563.
(39) Lemasters, J. J.; Holmuhamedov, E. Voltage-dependent anion channel (VDAC) as mitochondrial governator--thinking outside the box. *Biochim. Biophys. Acta* **2006**, *1762*, 181–190.
(40) Tikunov, A.; Johnson, C. B.; Pediaditakis, P.; et al. Closure of VDAC causes oxidative stress and accelerates the Ca(2+)-induced mitochondrial permeability transition in rat liver mitochondria. *Arch. Biochem. Biophys.* **2010**, *495*, 174–181.
(41) Brand, M. D.; Esteves, T. C. Physiological functions of the mitochondrial uncoupling proteins UCP2 and UCP3. *Cell Metab* **2005**, *2*, 85–93.
(42) Chan, C. B.; MacDonald, P. E.; Saleh, M. C.; et al. Overexpression of uncoupling protein 2 inhibits glucose-stimulated insulin secretion from rat islets. *Diabetes* **1999**, *48*, 1482–1486.
(43) Joseph, J. W.; Koshkin, V.; Zhang, C. Y.; et al. Uncoupling protein 2 knockout mice have enhanced insulin secretory capacity after a high-fat diet. *Diabetes* **2002**, *51*, 3211–3219.
(44) Dreyfuss, G.; Kim, V. N.; Kataoka, N. Messenger-RNA-binding proteins and the messages they carry. *Nat. Rev. Mol. Cell Biol.* **2002**, *3*, 195–205.
(45) Gao, F. H.; Wu, Y. L.; Zhao, M.; et al. Protein kinase C-delta mediates down-regulation of heterogeneous nuclear ribonucleoprotein K protein: involvement in apoptosis induction. *Exp. Cell Res.* **2009**, *315*, 3250–3258.
(46) Garayoa, M.; Man, Y. G.; Martinez, A.; et al. Downregulation of hnRNP A2/B1 expression in tumor cells under prolonged hypoxia. *Am. J. Respir. Cell Mol. Biol.* **2003**, *28*, 80–85.
(47) Zhao, C.; Zhang, W.; Tian, X.; et al. Proteomic analysis of cell lines expressing small hepatitis B surface antigen revealed decreased glucose-regulated protein 78 kDa expression in association with higher susceptibility to apoptosis. *J. Med. Virol.* **2010**, *82*, 14–22.
(48) Hossain, M. N.; Fuji, M.; Miki, K.; et al. Downregulation of hnRNP C1/C2 by siRNA sensitizes HeLa cells to various stresses. *Mol. Cell. Biochem.* **2007**, *296*, 151–157.
(49) Revil, T.; Pelletier, J.; Toutant, J.; et al. Heterogeneous nuclear ribonucleoprotein K represses the production of pro-apoptotic Bcl-xS splice isoform. *J. Biol. Chem.* **2009**, *284*, 21458–21467.
(50) Zhao, T. T.; Graber, T. E.; Jordan, L. E.; et al. hnRNP A1 regulates UV-induced NF-kappaB signalling through destabilization of cIAP1 mRNA. *Cell Death Differ.* **2009**, *16*, 244–252.
(51) Spahn, A.; Blondeau, N.; Heurteaux, C.; et al. Concomitant transitory up-regulation of X-linked inhibitor of apoptosis protein (XIAP) and the heterogeneous nuclear ribonucleoprotein C1-C2 in surviving cells during neuronal apoptosis. *Neurochem. Res.* **2008**, *33*, 1859–1868.
(52) Lee, J. N.; Zhang, X.; Feramisco, J. D.; et al. Unsaturated fatty acids inhibit proteasomal degradation of Insig-1 at a postubiquitination step. *J. Biol. Chem.* **2008**, *283*, 33772–33783.
(53) Liberek, K.; Lewandowska, A.; Zietkiewicz, S. Chaperones in control of protein disaggregation. *EMBO J.* **2008**, *27*, 328–335.
(54) Marzban, L.; Rhodes, C. J.; Steiner, D. F.; et al. Impaired NH2-terminal processing of human proislet amyloid polypeptide by the prohormone convertase PC2 leads to amyloid formation and cell death. *Diabetes* **2006**, *55*, 2192–2201.
(55) Vaughan, P. S.; Leszyk, J. D.; Vaughan, K. T. Cytoplasmic dynein intermediate chain phosphorylation regulates binding to dynactin. *J. Biol. Chem.* **2001**, *276*, 26171–26179.
(56) Gundersen, G. G.; Cook, T. A. Microtubules and signal transduction. *Curr. Opin. Cell Biol.* **1999**, *11*, 81–94.
(57) Pleasure, I. T.; Black, M. M.; Keen, J. H. Valosin-containing protein, VCP, is a ubiquitous clathrin-binding protein. *Nature* **1993**, *365*, 459–462.
(58) Pfeffer, S. R. Transport vesicle docking: SNAREs and associates. *Annu. Rev. Cell Dev. Biol.* **1996**, *12*, 441–461.